CHINESE OPTICS LETTERS

Vol. 22, No. 1 | January 2024

Mid-wavelength nBn photodetector with high operating temperature and low dark current based on InAs/InAsSb superlattice absorber

Peng Cao (曹 澎)[1,2], Tiancai Wang (王天财)[1,3], Hongling Peng (彭红玲)[1,4], Zhanguo Li (李占国)[5], Qiandong Zhuang[6], and Wanhua Zheng (郑婉华)[1,2,3,4*]

[1] Laboratory of Solid-State Optoelectronics Information Technology, Institute of Semiconductors, Chinese Academy of Sciences, Beijing 100083, China

[2] Center of Materials Science and Optoelectronics Engineering, University of Chinese Academy of Sciences, Beijing 100049, China

[3] College of Electronic and Communication Engineering, University of Chinese Academy of Sciences, Beijing 100049, China

[4] State Key Laboratory on Integrated Optoelectronics, Institute of Semiconductors, Chinese Academy of Sciences, Beijing 100083, China

[5] School of Physics, Changchun Normal University, Changchun 130022, China

[6] Physics Department, Lancaster University, Lancaster LA1 4YB, UK

*Corresponding author: whzheng@semi.ac.cn

Received August 4, 2023 | Accepted September 13, 2023 | Posted Online January 18, 2024

In this paper, we demonstrate nBn InAs/InAsSb type II superlattice (T2SL) photodetectors with AlAsSb as the barrier that targets mid-wavelength infrared (MWIR) detection. To improve operating temperature and suppress dark current, a specific Sb soaking technique was employed to improve the interface abruptness of the superlattice with device passivation using a SiO_2 layer. These result in ultralow dark current density of 6.28×10^{-6} A/cm^2 and 0.31 A/cm^2 under −600 mV at 97 K and 297 K, respectively, which is lower than most reported InAs/InAsSb-based MWIR photodetectors. Corresponding resistance area product values of $3.20 \times 10^4\ \Omega \cdot$ cm^2 and 1.32 $\Omega \cdot$ cm^2 were obtained at 97 K and 297 K. A peak responsivity of 0.39 A/W with a cutoff wavelength around 5.5 μm and a peak detectivity of 2.1×10^9 cm $\cdot$ Hz$^{1/2}$/W were obtained at a high operating temperature up to 237 K.

Keywords: mid-wavelength infrared photodetector; InAs/InAsSb superlattice; high operating temperature; dark current.
DOI: 10.3788/COL202422.012502

1. Introduction

Mid-wavelength infrared (MWIR) photodetectors play a crucial role in a wide range of applications, including gas detection, imaging, astronomy, science, and environmental monitoring[1–4]. However, the operating temperature is limited by significantly increasing dark current as the operating temperature rises, which is associated with the nature of the narrow bandgap the materials used. The dark current, typically due to the thermal excitation process, will rise exponentially as the temperature increases.

Over the past decades, many material systems have been exploited to work on MWIR spectra. Bulk narrowband gap InSb-based MWIR photodetectors are currently commercially mature, representing a dark current density of 1×10^{-9} A/cm^2 under −50 mV bias at 77 K[5]. Another commercially matured material option is HgCdTe (MCT). Simulation models were established[6,7] and experimental nBn type MCT devices have subsequently been realized with a saturation dark current about 0.54 A/cm^2 under −0.8 V at 180 K[8]. Moreover, narrow bandgap material InAs is also a candidate for MWIR detection. At room temperature, a dark current density of 2.5×10^{-2} A/cm^2 under −30 mV and a peak responsivity of 1.47 A/W were obtained from InAs-based devices[9]. A type II superlattice (T2SL) material system based on 6.1 Å (1 Å = 0.1 nm) lattice constant family (i.e. InAs/GaSb/AlSb) has also been utilized on the MWIR spectra. Interband cascade MWIR photodetectors based on InAs/GaSb superlattices have demonstrated a dark current of 3.6×10^{-7} A/cm^2 and 7.3×10^{-3} A/cm^2 under −5 mV bias at 77 and 295 K, respectively, with a responsivity of 0.167 A/W at 4 μm[10].

However, there are several drawbacks for the material system above that limit the optoelectronic performance of the devices. Less flexibility of tuning the bandgap for a wide spectral response is the main issue for the bulk materials InAs or

InSb, while the performance of HgCdTe-based MWIR photodetector devices is restricted by the nonuniform growth of large array and high cost CdZnTe substrate[11]. The T2SL InAs/GaSb system is a good candidate for MWIR detection, but the InAs/GaSb interfaces bring a strong scattering effect that shortens the photon-generated carriers' lifetime and increases dark current, resulting in a limitation on its operating temperature[12]. Thus, T2SL Ga-free InAs/InAsSb has been investigated since 2012 due to the potential long carrier lifetime of 412 ns[13]. Several attempts on improving the growth quality of InAs/InAsSb have been made to enhance the structural and optical properties of the InAs/InAsSb absorption layer[14]. As for the optoelectronic performance of InAs/InAsSb-based MWIR photodetectors, researchers at Northwestern University have optimized InAs/InAsSb-based MWIR photodetectors with an AlAsSb barrier in both planar and mesa configurations. These detectors demonstrated a dark current density of 0.44 A/cm^2 under −50 mV at 300 K and 2.5×10^{-2} A/cm^2 at 150 K[15,16]. Jiang *et al.* demonstrated an InAs/InAsSb-based photodetector with a cutoff wavelength of 3.5 μm, presenting a peak responsivity of 0.56 A/W under a reverse bias voltage of −130 mV[17]. Huang *et al.* proposed an MWIR photodetector using an InAs/InAsSb absorption layer and obtained a peak responsivity of 2.16 A/W at a temperature of 160 K[18]. Also, high-speed MWIR photodetectors exploiting higher p-doped InAs/InAsSb absorbers have been reported by Huang *et al.* that provide a large 3-dB bandwidth[19].

In this paper, we reported photodetectors with reduced dark current at higher temperatures using nBn type T2SL InAs/InAsSb MWIR photodetectors. This was achieved through the use of a lattice-matched AlAsSb layer as the electron barrier, which provides a large conduction band offset (CBO) between the InAs/InAsSb absorption layer and the barrier layer, employing an Sb soaking technique to improve the T2SL interfaces, which lowers the Shockley–Read–Hall (SRH)-related recombination current, and using a SiO_2 layer for passivation to suppress the surface leakage current that is related to dangling bonds.

2. Growth and Fabrication

To target MWIR photodetection, we employed a strain-balanced structure of $(3n, n) - InAs/InAs_{0.6}Sb_{0.4}$ T2SL (n is the thickness of InAsSb, while $3n$ is the thickness of InAs)[20]. The structure was grown on an n-GaSb substrate by molecular beam epitaxy (MBE). After the deposition of a 200 nm n-GaSb buffer layer, a 200 nm thick heavily n-doped InAs/InAsSb bottom contact layer was deposited, followed by a 1 μm thick unintentionally doped InAs/InAsSb T2SL layer. Then an undoped 10 nm-AlAsSb lattice matched to GaSb was grown, followed by a top contact layer of heavily n-doped InAs/InAsSb T2SL with narrower period thickness, which has wider bandgap energy acting as a window layer as well. The growth condition was set at a pre-optimized temperature of 400°C–430°C with a growth rate of 1 μm/h and a beam equivalent pressure (BEP) of 3×10^{-6} mbar for Sb. An Sb soaking technique that we developed previously was applied to improve the interfaces of the T2SL[21]. After the growth of InAs, both In and As shutters closed for 20 s to purge residual As; then 3 s later, Sb was deposited and followed by immediate growth of InAsSb. The mesa was dry-etched by an inductive coupled plasma (ICP) instrument, and then a 400 nm thick SiO_2 passivation layer was deposited over the sidewall by plasma-enhanced chemical vapor deposition (PECVD).

Figure 1 shows the high-resolution X-ray diffraction (HRXRD) pattern, which indicates the crystalline quality of the epilayer materials. The narrow superlattice 0th peak with a full width at half-maximum (FWHM) of 62 arcsec indicates an extremely high crystalline quality of InAs/InAsSb superlattice and abrupt interfaces.

Furthermore, the small angular separation between the superlattice *0*th peak and the GaSb substrate reflects the well strain-balanced InAs/InAsSb superlattice with respect to the GaSb substrate. As shown in Fig. 1, this angular separation value is found to be about 126 arcsec, which leads to a lattice mismatch of 0.10% according to Eq. (1)[22]. This indicates the InAs/InAsSb absorption layer is closely lattice matched to GaSb,

$$\Delta a/a = (\sin(\theta_{\text{substrate}})/\sin(\theta_{\text{substrate}} + \Delta\theta)) - 1, \qquad (1)$$

where $\Delta\theta$ stands for the angular separation between the epilayer and the substrate.

The simulation result reveals the T2SL has a structure of 48 Å − InAs/11 Å − $InAs_{0.62}Sb_{0.38}$.

Figure 2(a) shows the simulation results of the 48 Å − InAs/11 Å − $InAs_{0.62}Sb_{0.38}$ T2SL band diagram using SILVACO TCAD 2022 software. It reveals a cutoff wavelength at about 5.9 μm at 300 K, which covers the important atmospheric window of 3–5 μm and a spectral range that gives strong absorption to most molecules.

The schematic configuration of the fabricated mesa type nBn InAs/InAsSb device is shown in Fig. 2(b). The scanning electron microscope (SEM) image of the passivated mesa sidewall and the microscope image of the device are shown in Figs. 2(c) and 2(d), respectively.

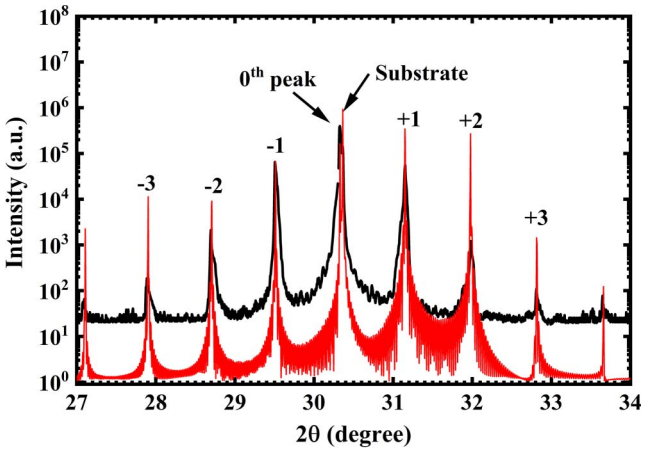

Fig. 1. HRXRD curve of InAs/InAsSb superlattice grown on GaSb substrate.

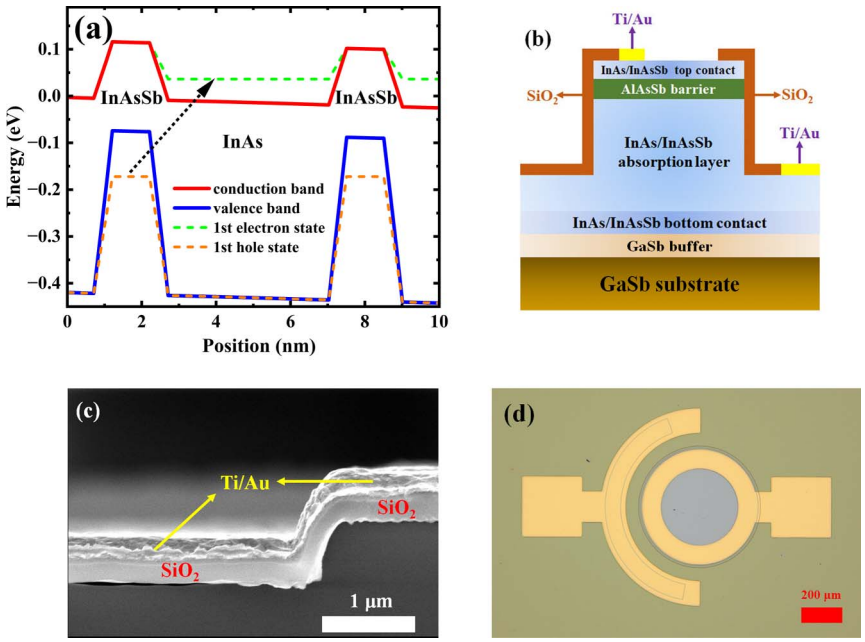

Fig. 2. (a) Band diagram of InAs/InAsSb superlattice; (b) schematic of fabricated InAs/InAsSb nBn device; (c) SEM image of passivated mesa sidewall of the device; (d) microscope image of the InAs/InAsSb nBn device.

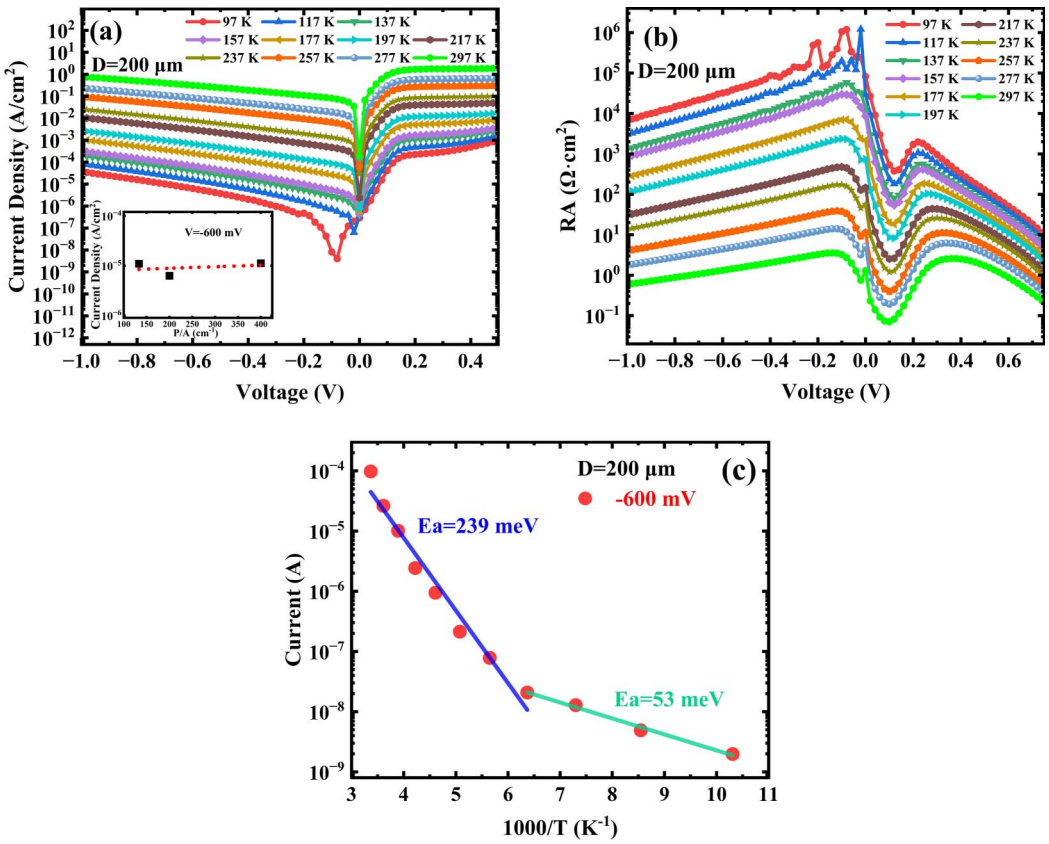

Fig. 3. Temperature dependent (a) dark current and (b) RA characteristic of 200 μm diameter InAs/InAsSb nBn device. The inset of (a) is the dark current density as a function of perimeter-to-area ratio (P/A). (c) Arrhenius plot of 200 μm diameter InAs/InAsSb nBn device under reverse bias of −600 mV.

3. Device Characteristic and Discussion

Temperature-dependent dark current characteristics and the differential resistance area product (RA) of a 200 μm diameter InAs/InAsSb nBn device are shown in Figs. 3(a) and 3(b). At 97 K, the device shows a dark current density of 6.28×10^{-6} A/cm^2 and an RA of $3.20 \times 10^4\ \Omega \cdot \text{cm}^2$ under a bias of −600 mV. At 297 K, under −600 mV, the dark current density increased to 0.31 A/cm^2 and a reduced RA of $1.32\ \Omega \cdot \text{cm}^2$ was obtained under similar bias. The inset of Fig. 3(a) represents the dark current density under −600 mV as a function of perimeter to area ratio (P/A) according to Ref. [23]. The dark current density shows an ultraweak dependence on the detector size, leading to an ultralow extracted surface current density. This is associated with the precisely controlled ICP etching process and the high quality of the densely deposited SiO_2 passivation layer over the mesa sidewall. Figure 3(c) shows the Arrhenius plot of the photodetector under a reverse bias of −600 mV. The extracted activation energy E_a of 239 meV can be concluded in the temperature range of 157 to 297 K. This is close to the energy bandgap of the designed InAs/InAsSb superlattice structure, which reveals that diffusion current dominates the whole dark current in the temperature range. At lower operating temperatures, e.g. from 157 to 97 K, E_a reduces to 53 meV, indicating a tunneling dark current component dominates in this temperature range. This suggests that the generation-recombination (G-R) current is eliminated due to the nBn structure.

Table 1 summarizes the dark current characteristics of InAs/InAsSb MWIR devices from several research works; our InAs/InAsSb nBn MWIR photodetectors demonstrate an ultralow dark current density compared to that of other groups.

Figure 4 shows the spectral photoresponse under different reverse biases at 237 K. A cutoff wavelength of 5.5 μm that is consistent with the bandgap simulation was obtained for this nBn InAs/InAsSb device. With the increasing reverse bias, the photoresponse increases simultaneously and nearly saturates at a reverse bias voltage of around −600 mV. A peak responsivity of 0.39 A/W was obtained at 237 K.

Table 1. Dark Current Characteristics of Different Reported InAs/InAsSb MWIR Photodetectors.

Ref.	D_{pixel} (μm)	Dark Current Density at High Temperature (A/cm^2)
[15]	100–400	0.44 (−50 mV, 300 K)
[17]	500	0.50 (−130 mV, 300 K)
[24]	50	0.865 (−100 mV, 300 K)
[25]	N/A	0.39 (−120 mV, 300 K)
[26]	20	3.94 (−1 V, 300 K)
This work	200	0.31 (−600 mV, 297 K)

Note: D_{pixel} is the diameter of the InAs/InAsSb MWIR photodetector device.

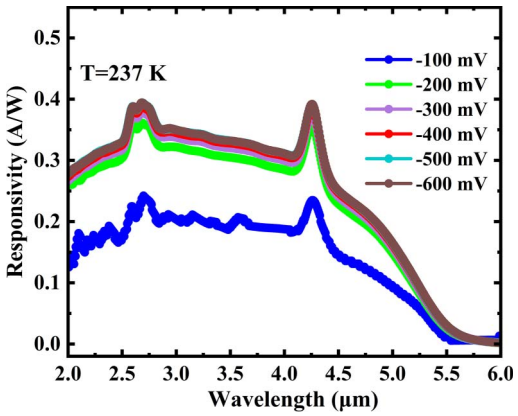

Fig. 4. Photoresponse varying with reverse bias voltage at 237 K.

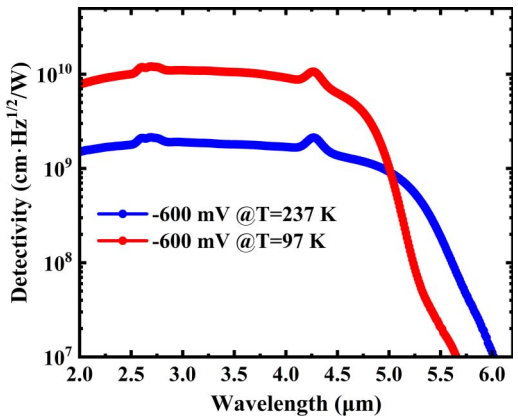

Fig. 5. Detectivity of nBn InAs/InAsSb device at 97 and 237 K.

Figure 5 shows the calculated detectivity of this nBn InAs/InAsSb photodetector device under reverse bias voltage of −600 mV at an operating temperature of 97 and 237 K, respectively. At 97 K, the peak detectivity is about $1.2 \times 10^{10}\ \text{cm} \cdot \text{Hz}^{1/2}/\text{W}$, while peak detectivity decreases to $2.1 \times 10^9\ \text{cm} \cdot \text{Hz}^{1/2}/\text{W}$ as the temperature rises up to 237 K.

4. Conclusion

In summary, we demonstrated nBn T2SL InAs/InAsSb MWIR photodetectors containing an AlAsSb electron barrier with several attempts to suppress dark current density and increase operating temperature. An ultralow dark current density of 6.28×10^{-6} A/cm^2 and 0.31 A/cm^2 was obtained under reverse bias −600 mV at 97 and 297 K, respectively. This dark current density level is lower than that of the reported InAs/InAsSb MWIR photodetectors, to the best of our knowledge. The device under study showed a cutoff wavelength of 5.5 μm. Also, peak responsivity of 0.39 A/W and peak detectivity of $2.1 \times 10^9\ \text{cm} \cdot \text{Hz}^{1/2}/\text{W}$ were obtained of this nBn InAs/InAsSb device at a high operating temperature of up to 237 K.

Acknowledgements

This work was supported by the National Science and Technology Major Project (No. 2018YFE0200900).

References

1. Y. Liu, Q. Yang, J. Liu, *et al.*, "MWIR imaging experiments with large *F*-number optics on LEO spacecraft," Infrared Phys. Technol. **67**, 315 (2014).
2. Z. Wu and X. Wang, "Non-uniformity correction for medium wave infrared focal plane array-based compressive imaging," Opt. Express **28**, 8541 (2020).
3. S. Thibault, V. N. Mahajan, R. B. Johnson, *et al.*, "Development of the infrared instrument for gas detection," Proc. SPIE **10375**, 103750R (2017).
4. K. Cawse-Nicholson, P. A. Townsend, D. Schimel, *et al.*, "NASA's surface biology and geology designated observable: a perspective on surface imaging algorithms," Remote Sens. Environ. **257**, 112349 (2021).
5. A. Evirgen, J. Abautret, J. P. Perez, *et al.*, "Midwave infrared InSb nBn photodetector," Electron. Lett. **50**, 1472 (2014).
6. A. M. Itsuno, J. D. Phillips, and S. Velicu, "Design and modeling of HgCdTe nBn detectors," J. Electron. Mater. **40**, 1624 (2011).
7. M. Kopytko, "Design and modelling of high-operating temperature MWIR HgCdTe nBn detector with n- and p-type barriers," Infrared Phys. Technol. **64**, 47 (2014).
8. A. M. Itsuno, J. D. Phillips, and S. Velicu, "Mid-wave infrared HgCdTe nBn photodetector," Appl. Phys. Lett. **100**, 161102 (2012).
9. H. Lin, Z. Zhou, H. Xie, *et al.*, "High-performance room-temperature extended-wavelength InAs-based middle-wavelength infrared photodetector," Phys. Status Solidi A **218**, 2100281 (2021).
10. N. Gautam, S. Myers, A. V. Barve, *et al.*, "High operating temperature interband cascade midwave infrared detector based on type-II InAs/GaSb strained layer superlattice," Appl. Phys. Lett. **101**, 021106 (2012).
11. E. Plis, B. Klein, S. Myers, *et al.*, "High operating temperature midwave infrared InAs/GaSb superlattice photodetectors on (111) GaSb substrates," IEEE Electron Device Lett. **34**, 426 (2013).
12. S. P. Svensson, D. Donetsky, D. Wang, *et al.*, "Growth of type II strained layer superlattice, bulk InAs and GaSb materials for minority lifetime characterization," J. Cryst. Growth **334**, 103 (2011).
13. T. Schuler-Sandy, S. Myers, B. Klein, *et al.*, "Gallium free type II InAs/$InAs_xSb_{1-x}$superlattice photodetectors," Appl. Phys. Lett. **101**, 071111 (2012).
14. B. Liu, L. Zhu, Y. Liu, *et al.*, "Temperature dependent growth of InAs/InAsSb superlattices by molecular beam epitaxy for HOT mid-wavelength infrared detectors," Mater. Sci. Semicond. Process. **163**, 107590 (2023).
15. D. Wu, J. Li, A. Dehzangi, *et al.*, "Mid-wavelength infrared high operating temperature pBn photodetectors based on type-II InAs/InAsSb superlattice," AIP Adv. **10**, 025018 (2020).
16. A. Dehzangi, D. Wu, R. McClintock, *et al.*, "Demonstration of planar type-II superlattice-based photodetectors using silicon ion-implantation," Photonics **7**, 68 (2020).
17. J. Jiang, G. Wang, D. Wu, *et al.*, "High-performance infrared photodetectors based on InAs/InAsSb/AlAsSb superlattice for 3.5 microm cutoff wavelength spectra," Opt. Express **30**, 38208 (2022).
18. J. Huang, S. Yan, T. Xue, *et al.*, "Mid-wavelength InAs/InAsSb superlattice photodetector with background limited performance temperature higher than 160 K," IEEE Trans. Electron Devices **69**, 4392 (2022).
19. J. Huang, Z. Dai, Z. Shen, *et al.*, "High-speed mid-wave infrared InAs/InAsSb superlattice uni-traveling carrier photodetectors with different absorber doping," IEEE Trans. Electron Devices **69**, 6890 (2022).
20. D. Z. Ting, S. B. Rafol, A. Khoshakhlagh, *et al.*, "InAs/InAsSb type-II strained-layer superlattice infrared photodetectors," Micromachines **11**, 958 (2020).
21. A. Krier, M. Stone, Q. D. Zhuang, *et al.*, "Mid-infrared electroluminescence at room temperature from InAsSb multi-quantum-well light-emitting diodes," Appl. Phys. Lett. **89**, 091110 (2006).
22. P. Christol, F. de Anda, V. Compean, *et al.*, "Antimonide-based superlattice infrared barrier photodetectors," in *Proceedings of the 8th International Conference on Photonics, Optics and Laser Technology* (2020), p. 45.
23. Y. Teng, X. Hao, H. Zhu, *et al.*, "Demonstration of MOCVD-grown long-wavelength infrared InAs/GaSb superlattice focal plane array," IEEE Access **9**, 60689 (2021).
24. E. Delli, V. Letka, P. D. Hodgson, *et al.*, "Mid-infrared InAs/InAsSb superlattice nBn photodetector monolithically integrated onto silicon," ACS Photonics **6**, 538 (2019).
25. D. Wu, J. Li, A. Dehzangi, *et al.*, "High performance InAs/InAsSb type-II superlattice mid-wavelength infrared photodetectors with double barrier," Infrared Phys. Technol. **109**, 103439 (2020).
26. J. Huang, Z. Shen, Z. Wang, *et al.*, "High-speed mid-wave infrared uni-traveling carrier photodetector based on InAs/InAsSb type-II superlattice," IEEE Electron Device Lett. **43**, 745 (2022).